Pergamon

Acta mater. Vol. 46, No. 7, pp. 2431–2439, 1998

Printed in Great Britain
PII: S1359-6454(97)00401-1
1359-6454/98 $19.00 + 0.00

HIGH RESOLUTION AND ENERGY FILTERING TEM STUDY OF INTERFACIAL STRUCTURE AND REACTION IN ADVANCED MATERIALS PROCESSING

HOLIN CHANG[1], L. CHANG[2], FU-RONG CHEN[1], J. J. KAI[1], EUGENE TZOU[3], JIANMING FU[3], ZHENG XU[3], J. EGERMEIER[3] and FU-SEN CHEN[3]

[1]Center of Electron Microscopy/Department of Engineering and System Science, National Tsing Hua University, Hsinchu, Taiwan, [2]Department of Materials Science and Engineering, National Chiao-Tung University, Taiwan and [3]Applied Materials, Inc., PVD Products Business Group, Santa Clara, CA, U.S.A.

Abstract—High resolution TEM becomes more powerful when coupled with a Gatan imaging filter (GIF). It gives both structural and compositional information simultaneously with subnanometer and nanometer resolution, respectively. By means of these combined techniques, the failure mechanism of diffusion barrier layers in IC devices, having the structure of Al–1%Si–0.5%Cu/TiN/Ti/Si substrate, was investigated. In non-oxygen stuffed samples thermally stressed at 550°C for 1 h, serious Al spikes below contacts were observed where metal layer Ti also reacted with Si substrate to form C49–$TiSi_2$ and was consumed completely. TiN and Al become unstable due to high temperature thermal stress and reacted into $TiAl_3$ and AlN. Decomposition of TiN degraded the function of the barrier layer, and so a diffusion path at the weakest point of the contact corner was opened for metal Al alloy to diffuse through the barrier layer and to form a spike below the TiN layer. We also showed that the oxygen-stuffing processes after each TiN/Ti deposition enhances the barrier capability against Al/Si diffusion in thermal stress. It was found that Ti and TiN were oxidized to form titanium oxide which reacted with the Al alloy. As a result, Al_2O_3 and $TiAl_3$ were found above the TiN layer. Therefore, it is concluded that oxidation during oxygen-stuffing processes provides a means to inhibit diffusion in thermal stress processes, and maintains integrity of the stack structure. © *1998 Acta Metallurgica Inc.*

1. INTRODUCTION

TiN is widely used as a diffusion barrier layer between Al contact and Si substrate in VLSI metallization and contact technology because of its attractive properties, such as electrical conductivity, high thermal stability, resistance to diffusion of Al and Si, and a simple manufacturing process [1]. In order to reduce contact resistance and promote adhesion, a layer of pure Ti is deposited between TiN and Si substrate in the form of TiN/Ti/Si [2]. Finally, the contact holes are metallized by Al alloy to connect current circuits. However, TiN becomes active when it contacts with Al at high temperature, resulting in the degradation of TiN and a spike formed below the barrier layer. Eventually, device failure occurs [3–8]. It is a severe reliability problem in high temperature processes which require annealing treatment to reduce contact resistance as VLSI circuit dimensions approach sub-micrometer size [1]. "Thermal stress test" is a term used by IC process for such annealing treatments, and will be used in this paper. This paper deals with structural and compositional evolution at interfaces of TiN/Ti diffusion barrier layer with Al contact and Si substrate after thermal stress test, trying to understand the possible reactions at high temperature and the failure mechanism in more detail.

It is well-known that the physical properties of materials are frequently influenced by the structure and chemistry of interfaces. For example, a small amount of bismuth segregating to the grain boundary of copper causes embrittlement [9]. ZnO can be used as a varistor by controlling appropriate additives in grain boundaries of ZnO to modify the energy band structure near the boundaries [10]. Similarly, chemical reaction at interfaces will play an important role in VLSI technology, in which case the electrical properties contributed by interfaces of thin films may have a significant impact on the performance of the bulk structure. High resolution transmission electron microscopy (HRTEM) has been a very powerful technique to reveal the atomic structure of grain boundaries and interfaces in the past decades [11–14]. However, HRTEM provides little information about the compositions in the materials and therefore only offers incomplete correlation with the properties of materials. The interaction of fast incident electron beam with the atomic electrons of the sample results in inelastic processes that lead to energy losses. Electron energy-loss spectroscopy (EELS) contains fruitful information on compositions, as shown by the characteristic edges of energy loss. In recent years, a commercial post-column energy filter (or image filter) has been available to image two-dimensional

distribution of a particular element by selecting particular energy losses of inelastic electrons with an energy slit [15]. The energy filter mainly consists of an electron energy-loss spectrometer in the front part and an imaging lens system in the back. Combination of the image filter with a field-emission gun TEM (FEG TEM) provides not only structural information at atomic resolution, but also the two-dimensional distribution of composition at near nanometer resolution [16]. We present results from FEG TEM with energy filter and energy dispersive spectrometer of X-ray (EDX) to reveal the interfacial reaction of contact metal Al with TiN/Ti barrier layer in a submicron diode barrier test. All the energy filtered images were acquired through a Gatan image processing software named "Digital Micrograph".

2. EXPERIMENT

The samples for the present investigation were prepared by the Endura 5500 system of Applied Materials. There were two different dimensions of contact holes for analysis, 0.8 or 0.6 μm wide and 1.2 μm deep. The stack structure with diffusion barrier layer was Al–1%Si–0.5%Cu/TiN 100 nm/Ti 20 nm/Si substrate. Titanium was deposited on Si substrate by physical vapor deposition at 100°C and titanium nitride was deposited by reactive sputtering at 400 °C. In order to improve step coverage, a collimator was employed in the deposition of titanium and titanium nitride. Two different process conditions were applied on two wafers, one is called OS sample with oxygen stuffing and the other is called NOS sample without oxygen stuffing. The process steps of OS samples were: deposition of Ti, *in situ* oxygen stuffing in N_2–5%O_2 atmosphere for 30 s, deposition of TiN, *in situ* oxygen stuffing in N_2–5%O_2 atmosphere for 30 s and then Al planization at 400°C. The NOS one followed the steps in similar conditions: deposition of Ti, TiN, *in situ* anneal in N_2 and Al alloy planization. After a thermal stress test at 550°C for 1 h, all NOS samples failed, while OS samples had no failure. Figure 1 is a schematic diagram showing the expected structure of a NOS contact before thermal stress test.

Cross-sectional TEM specimens were prepared using a special technique developed by Hong Zhang [17]. This technique allows us to produce a very thin TEM specimen near a particular interconnect to obtain HRTEM images and core-loss filtered images for Si, Ti, N, O, and Al elements. In energy filtering, the image acquired beyond and before an ionization edge is called as the post-edge image and pre-edge image, respectively. A two-windows method for imaging the distribution of particular elements as composition map has been adopted, in which the post-edge image is simply divided by the pre-edge image [16, 18, 19]. In general, this method is fast and useful for qualitative analysis but does not relate directly to the elemental concentration. The compositional map obtained using such a two-windows technique provides information about the distribution of the elements in the sample according to the intensity in the image. Darker contrast in a compositional map presents relative lower concentration of the elements. The compositional image obtained by this method is therefore called ratio map. However, it is believed that compositional map obtained by the ratio mapping technique shows less dynamical diffraction contrast than the three-window method [19]. In our experiment, the elemental maps for Al, Si, N, Ti, and O were acquired at core loss energy of 73, 99, 401, 456, and 532 eV, respectively, with the width of the energy slit of 5 eV for aluminum, 10 eV for silicon, 20 eV for nitrogen, 40 eV for titanium, and 30 eV for oxygen. Acquisition time for each map varies from 2 to 40 s, depending on the intensity of core loss signals. Specimen drift was not noticeable during image acquisition. One difficulty in this research is making IC contact specimen very thin, otherwise high background from low loss region may obscure the L-edge signals of Al and Si. In order to minimize the contribution of the background in the energy loss region less than 100 eV and overlapping of the extended L-edges of Al

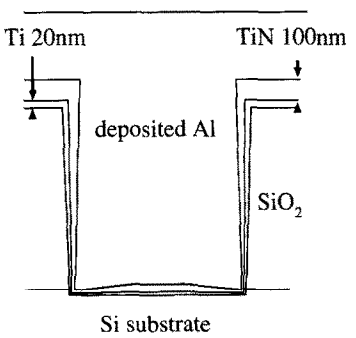

Fig. 1. A schematic of the expected structure from the non-oxygen stuffing process before the thermal stress test.

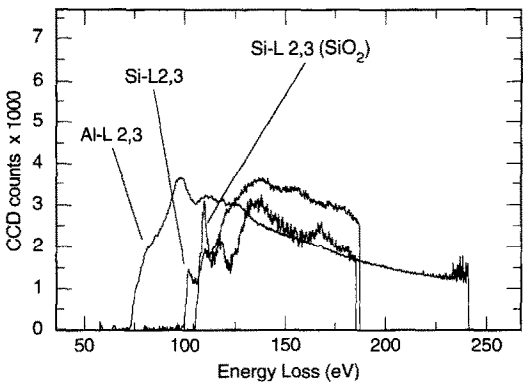

Fig. 2. Spectra of L-edges associated with Al, Si and SiO_2.

beyond 100 eV with Si L-edge, the energy silt of 5 and 10 eV was used to acquire Al and Si maps, respectively. Spectra of L-edges associated with Al, Si and SiO_2 are shown in Fig. 2. The positions of the energy slit used for obtaining Si map is also given in the spectra. The following considerations should be taken into account to interpret the mapping results correctly. Since the onset of Si L-edge in the SiO_2 is at 110 eV, signals of Si in SiO_2 may not correspond to the composition ratio in Si map. Also, the effect of Al L-edge signals on Si mapping is not completely avoidable. Furthermore, although the two windows technique could minimize diffraction contrast comparing the three windows technique, we have found that the diffraction contrast is still noticeable in this energy regime. We will discuss these issues in the next section. The FEG TEM in our laboratory is a JEOL JEM 2010F equipped with an Oxford energy-dispersive X-ray spectrometer and a Gatan Imaging Filter (GIF). All EDX spectra were obtained by a nanoprobe electron beam with a diameter of 1 nm.

3. RESULTS AND DISCUSSION

Figure 3 shows a typical TEM image of a 0.8 μm contact with oxygen-stuffing barrier layer after the test of thermal stress. Basically, the TiN layer has a columnar structure. The different image contrast shows that there are a few layers at barrier location of deposited TiN and Ti. One of the layers is between the contact metal Al (Si, Cu) and barrier. Figures 4(a) and (b) shows images at two different locations in a NOS sample. There are some common interesting features in these two images where spikes occurred. In Fig. 4(a) under the barrier, there is a large spike with triangular shape in a size of about 500 nm. Within the triangular spike there are some small spikes in half circle shape having size of about 50 nm. No such spikes in Si substrate was observed in OS samples. We will first discuss

Fig. 3. Typical TEM bright field image of a 0.8 μm contact with an oxygen-stuffing barrier layer after the test of thermal stress.

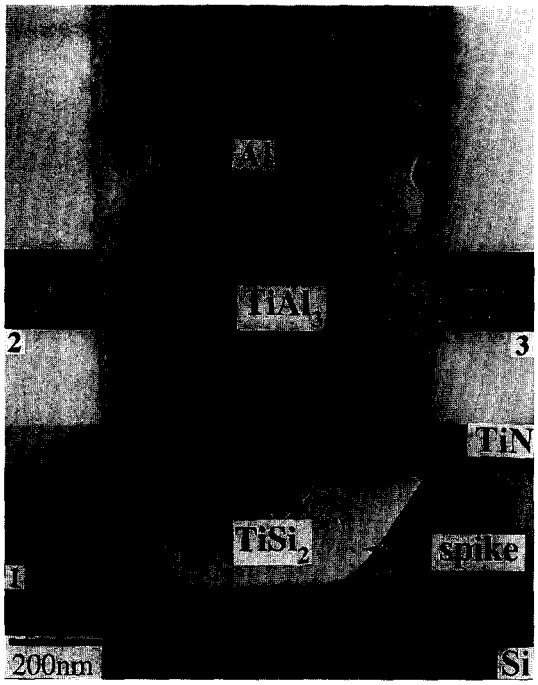

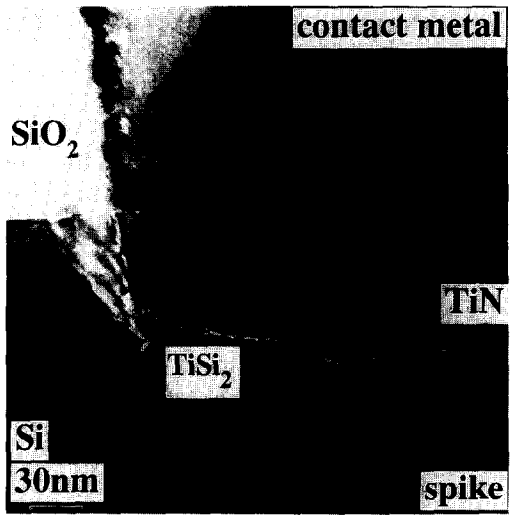

Fig. 4. (a) and (b) are images at two different locations where a spike occurred in a NOS sample.

the energy-filtering, EDX and HRTEM analyses of the NOS samples, and then compare the results with those of the OS samples.

3.1. NOS sample

Figures 5(a) to (f) show a set of zero loss and elemental maps for O, Si, N, Ti and Al, respectively, from the left corner of the contact in Fig. 4(a). All compositional maps are aligned with reference to the particular common features such as the shape of the barrier in each map with Digital Micrograph. These maps are shown as acquired experimentally without being processed by using any image processing software. All the images have the same magnification as shown in the zero loss image. The O

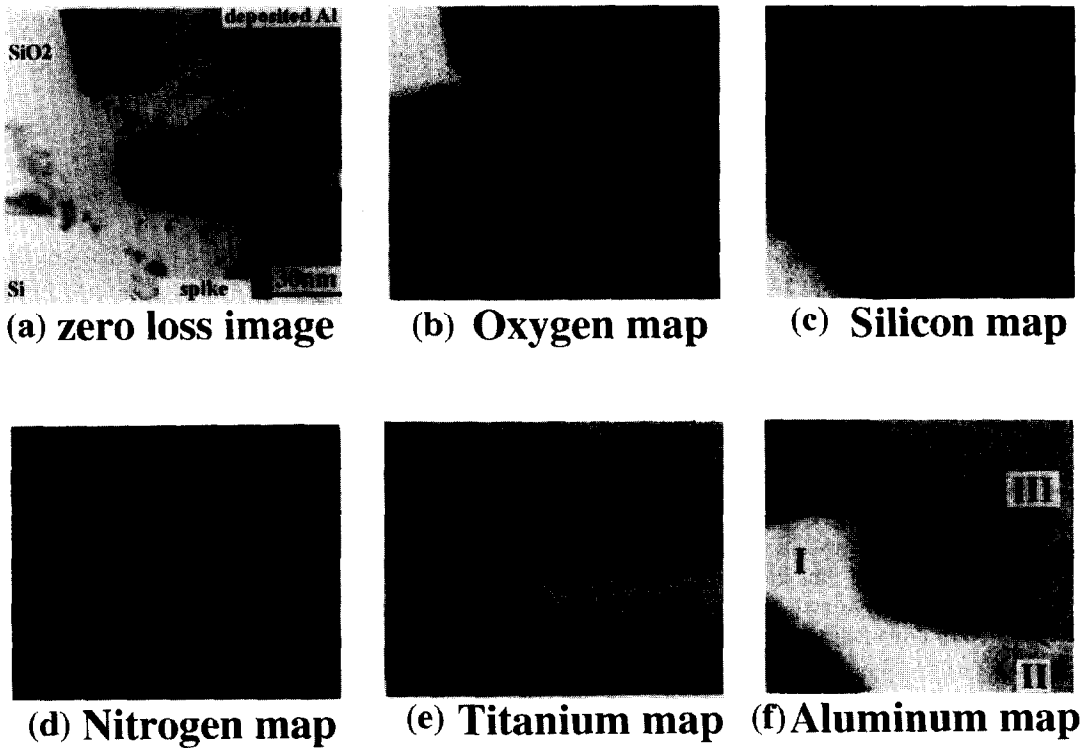

Fig. 5. (a) Zero loss image, (b) O, (c) Si, (d) N, (e) Ti and (f) Al map, respectively, from the left corner of the contact in Fig. 4(a). All the images have the same magnification as shown in the zero loss image.

map in Fig. 5(b) shows the area of SiO_2. The weak bright contrast in contact metal Al(Si, Cu) and silicon regions of the O map may arise from surface oxides. The Si map was acquired with 10 eV energy slit at 105 and 90 eV for post- and pre-edge images. In the Si map of Fig. 5(c), the Si substrate exhibits bright contrast, while the triangle region and contact metal Al have a grey color. SiO_2 in the Si map shows darkest contrast because the energy slit did not cover beyond 115 eV which is the onset of Si L-edge of SiO_2. It was mentioned earlier that the Si maps may display complicated contrast due to the fact that the Al signal may contribute to the Si map and the small energy slit may not include the right portion of the signal for Si and SiO_2. Thus, the Si map may not give the correct compositional distribution where the contact metal Al and the truncated triangle area have higher intensity than SiO_2 area. This point will become more clear in a later discussion about an EDX analysis where the truncated triangle area contains actually near pure Al(Si) referred to as region I, a half circle area within the triangle referred to as region II, and the contact metal $Ti(Al_{0.8}\ Si_{0.2})_3$ near the bottom of contact referred to as region III close to the $TiAl_3$ alloy. The regions I, II and III are marked in the Al map of Fig. 5(f) since this map clearly reveals all three regions.

Within the triangle area, a small spike with a half circle shape and a size of about 50 nm was found in the Si substrate. Reminding that Fig. 5 is a part of Fig. 4(a), only a part of the half circle can be seen in Fig. 5(e) and (f). This half circle spike was marked as "region II". The regions II and III show bright contrast in both Ti [Fig. 5(e)] and Al maps [Fig. 5(f)] which implies that these two regions contain titanium and aluminum elements. The compositional information from each region I, II and III can be obtained complementarily from EDX spectra in the nano-beam mode using the Cliff–Lorimer thin-film criterion [20, 21]. The triangle spike of region I contains almost pure Al with small amount of silicon. The half-circle area (region II) has a composition ratio close to $Ti(Si_{0.9}Al_{0.1})_2$, while the contact metal (region III) is close to $Ti(Al_{0.8}\ Si_{0.2})_3$. Further EDX analysis in the contact metal about 50 nm away from $Ti(Al_{0.8}Si_{0.2})_3$, shows that no titanium was detected and the Si atomic concentration was slightly higher than 1%. The formation of $Ti(Al_{0.8}Si_{0.2})_3$ occurs only at the interface between the contact metal and barrier. $Ti(Si_{0.9}Al_{0.1})_2$ has the same crystal structure as C49–$TiSi_2$ and little difference in lattice constant from that of C49–$TiSi_2$ [22]. A diffraction pattern obtained using a nano-beam from this small half circle spike (region II) is shown as an inset (1) in Fig. 4(a). This pattern can be indexed to be an axis of $[5\bar{3}\bar{1}]$. The region II shows a darker contrast in the Si map. This could be for the same reason as for SiO_2 where the onset of the Si L-edge of $TiSi_2$ may shift from that of Si.

$Ti(Al_{0.8}\ Si_{0.2})_3$ has the same crystal structure as Al_3Ti and also with little difference in lattice

parameters [22]. 20% of Al in compound $TiAl_3$ is replaced by Si to turn into $Ti(Al_{0.8}Si_{0.2})_3$. The nano-beam diffraction patterns from region III were also obtained and shown as insets (2) and (3) in Fig. 4(a). These two patterns were indexed to be $[82\bar{1}]$ and $[42\bar{1}]$, respectively.

The most interesting feature in the compositional maps is that the barrier layer is wider and continuous in the N map, while it is thinner and broken in the Ti map. It suggests that nitrogen might spread out after a thermal test at 550°C. The result is inconsistent with the expected stacking structure Al/TiN/Ti/Si in NOS sample (Fig. 1) in which the distribution of the titanium shall be wider than that of nitrogen. The spreading nitrogen and broken titanium in the barrier may imply that interfacial reaction occurred after the thermal stress test.

It was worth noting there are dark gaps between the half circle of the $Ti(Si_{0.9}Al_{0.1})_2$ and the barrier as well as between the barrier and the contact metal in Ti map. These gaps show bright contrast in N and Al maps which suggests that the gap areas could be AlN. Again these maps were aligned with the reference of the common features in these maps using the Digital Micrograph software. The formation of a titanium–aluminum alloy and AlN at 550°C is permitted, which can be explained from thermodynamics [23, 24]. The free energies of the reactions of Al and TiN could be written as follows [23]

$$2TiN + 7Al \longrightarrow 2AlN + Ti_2Al_5$$
$$\Delta G_1 = -19291.4 + 11.635T$$

$$TiN + 4Al \longrightarrow TiAl_3 + AlN$$
$$\Delta G_2 = -32753.6 + 11.08T$$

where T is the temperature in degree Kelvin. At 550°C, ΔG_1 is equal to −9.715 kJ and ΔG_2 is equal to −23.6 kJ.

It has been suggested that aluminum diffusing through the grain boundaries of the columnar TiN film is the cause for spiking in the Si substrate [25]. The grain boundary diffusivity from 300 to 550°C for aluminum in the TiN film of columnar grain structure had been determined to be [25]

$$D\ [m^2\ s^{-1}] = 3*10^{-18} \exp(-30/RT)$$

However, an *in-situ* TEM experiment showed that once Al began to penetrate through the TiN, Al spread widely in the Si substrate in just 2 s at 550°C [26]. A pure diffusion mechanism cannot be completely responsible for such a fast penetration of Al through the TiN layer, because it takes 30 min for Al in TiN to reach a mean penetration depth of 30 nm at 550°C with the diffusivity given above. An interfacial reaction must be cooperating to some extent during the thermal stress test. A ternary phase diagram indicates that the reaction products of TiN with Al at 600°C are Al_3Ti and AlN [27]. It has been reported that a ternary compound $Al_xTi_ySi_z$ could form at the TiN/Al interface [28]. A previous HRTEM work [26] had suggested that formation of nanocrystalline $TiAl_3$ in the Al/TiN interface could occur. However, no detailed analysis on the HRTEM image of nanocrystalline $TiAl_3$ was done in the previous work, the evidence for the existence of nanocrystalline $TiAl_3$ from the HRTEM image lacked certainty [26]. The real confirmation of the $TiAl_3$ phase was from an X-ray diffraction analysis [26]. In our experiment, we have observed the $Ti(Al_{0.8}Si_{0.2})_3$ phase which is close to the $TiAl_3$ phase from nano-beam diffraction and EDX analyses. The interfacial reaction of Al and TiN at high temperature to form AlN and $TiAl_3$ phases is conceivable from N, Ti and Al maps, diffraction patterns, and EDX analyses, and is supported by thermodynamics calculations.

Once Al penetrates through the TiN film in some area, usually near the junctions of SiO_2, Si and TiN/Ti barrier from many observations in our experiment, the above reaction takes place along the interface of Al/TiN/Si to form AlN and $TiAl_3$ phases. Since, at 550°C, the Al atoms are very mobile, non-reacted residual Al will move down fast to form a large spike containing almost pure aluminium with little amount of silicon dissolved, while the Ti metal barrier could react with Si substrate to form C49–$TiSi_2$ with a certain percentage of Al. Beware that interdiffusion of Ti, Si and Al may also accompany the interfacial reaction, so that the regions of the contact metal Al contain Ti and Si, while the TiN layer and half circle spike contain Al and Si. A schematic barrier structure after a thermal stress testing for the NOS sample in Fig. 4(a) can be concluded from the above analyses and is depicted in Fig. 6.

Figure 7 shows compositional maps of Fig. 4(b). Again, similar features in the compositional maps of Fig. 5 also appear in Fig. 7. The same analyses and considerations shown above were performed in

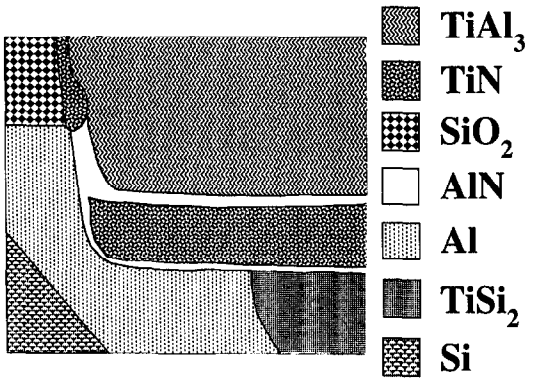

Fig. 6. A schematic barrier structure after a thermal stress testing for the NOS sample in Fig. 4(a).

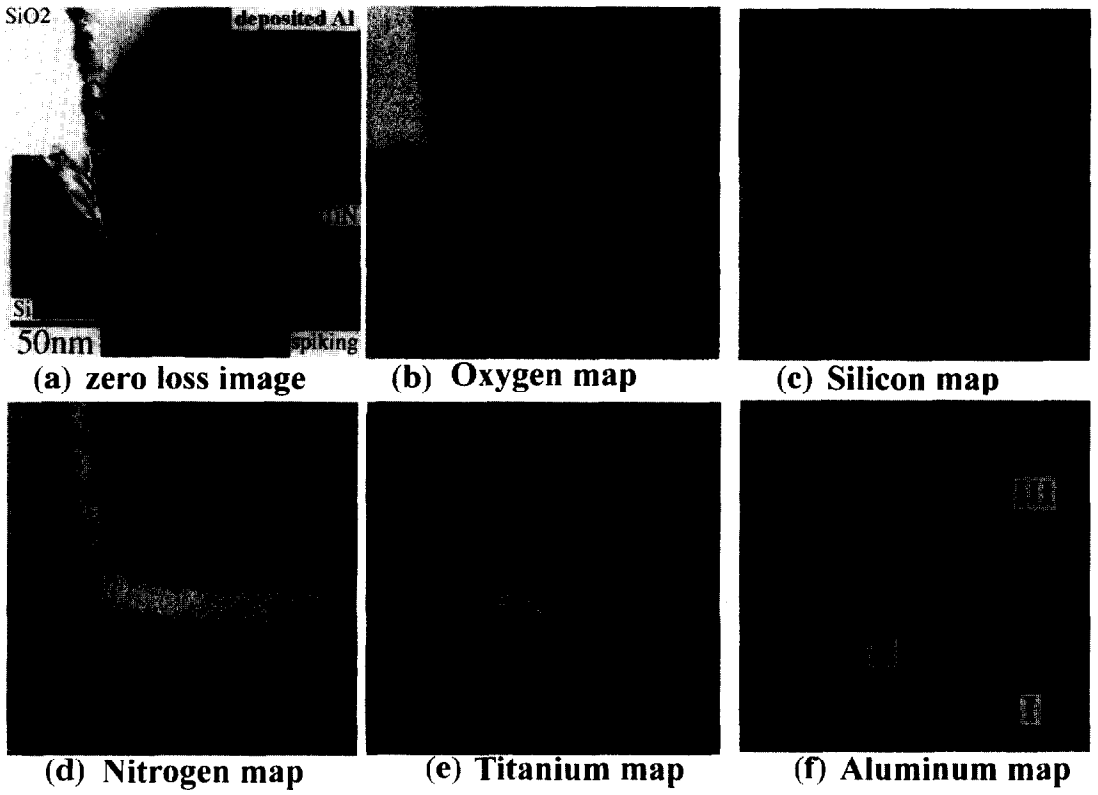

Fig. 7. (a) Zero loss image (b) O, (c) Si, (d) N, (e) Ti and (f) Al map, respectively, from the left corner of the contact in Fig. 4(b). All the images have the same magnification as shown in the zero loss image.

this case. Nitrogen spread out after the thermal test such that the distribution of nitrogen in the N map is wider than titanium, and the titanium is broken in the Ti map. Both of $Ti(Si_{0.9}Al_{0.1})_2$ and $Ti(Al_{0.8}Si_{0.2})_3$ were found in this NOS sample in the positions of spike and contact metal, respectively. The difference is that the $Ti(Si_{0.9}Al_{0.1})_2$ in region II is of trapezoid shape instead of half circle shape.

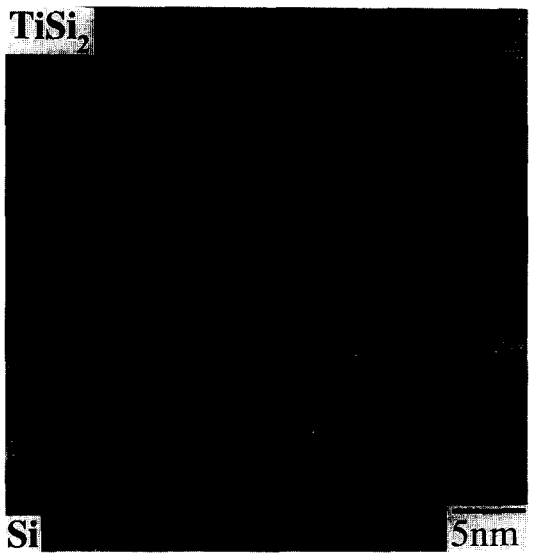

Fig. 8. A high resolution image of $Ti(Si_{0.9}Al_{0.1})_2$. The zone axis is [100].

The composition and structure in the trapezoid region were confirmed using nano-beam EDX and HRTEM. A high resolution image of this $Ti(Si_{0.9}Al_{0.1})_2$ is shown in Fig. 8. The zone axis of this high resolution image is [100] of C49–$TiSi_2$. The trapezoid region shows a darker contrast than the Si region. This could be due to the same reason as for SiO_2 as explained in the previous discussion. A dark gap also exists between the region II and the barrier layer. The resultant structure of this barrier can be deduced and is given in Fig. 9. These two examples above demonstrate that the Al and

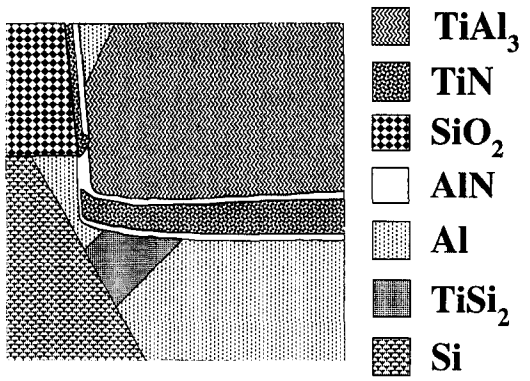

Fig. 9. A schematic barrier structure after thermal stress testing for the NOS sample in Fig. 4(b).

TiN reacting to form AlN and a titanium–aluminium alloy is common evidence and is responsible for the spiking in the device for NOS processing.

3.2. OS sample

Figure 10 is a set of O, Si, N, Ti and Al composition maps of the oxygen-stuffing barrier layer in an OS sample. The O map clearly shows two interfacial oxide layers which are consistent with the double oxygen stuffing processes. The top oxide layer is about 5 nm in thickness which is formed due to oxidation of the TiN layer. The lower oxide layer shows a strong oxygen signal within 5 nm, but it has a weak and long tail of oxygen signal extended further about 5 nm in thickness. Titanium is an oxygen-gettering material and oxide-reducing agent [3]. This may imply that the Ti layer may be oxidized to some extent during the oxygen stuffing process. It is interesting to note that no $TiSi_2$ was found from the Ti map just like the NOS sample described above, which may be due to the oxidation of the Ti layer to form TiO_x during the oxygen stuffing process. As shown in the N and Ti maps, the thickness of both N and Ti in the barrier layer remains the same as that before they were being thermally stressed. The most interesting feature in the Ti map is a dark gap between the contact metal and the barrier. The position of this dark gap in the Ti map coincides with a white band between the contact metal and the barrier in Fig. 10(a). Aligning these maps with reference to the common characteristics in each map using Digital Micrograph, we found that the region of the dark gap shows a bright signal in both O and Al maps. Intensity profiles across the interface and contact metal/barrier obtained from O, Al and Ti are given in Fig. 11. This may imply that interfacial reactions may occur. The possible reactions are proposed in the following:

The surface of TiN barrier may first oxidize to form the TiO_2:

$$TiN + O_2 \longrightarrow TiO_2 + 1/2N_2$$

$$\Delta G_3 = -0.57 \times 10^{-6} + 79.44T$$

At 400°C of oxygen stuffing, ΔG_3 is -0.52×10^6 kJ. The following reaction took place either during sputtering of Al at 400°C or the thermal test at 550°C.

$$TiO_2 + 13/2Al \longrightarrow TiAl_3 + 2/3Al_2O_3$$

$$\Delta G_4 = -203752.6 - 11.1 \log T + 69.55T$$

At 550°C, ΔG_4 is equal to -1.6×10^5 kJ. From the viewpoint of thermodynamics, formation of a Al_2O_3 interfacial layer between the contact metal and barrier is much more favorable since the free energies of the two reactions above are very low.

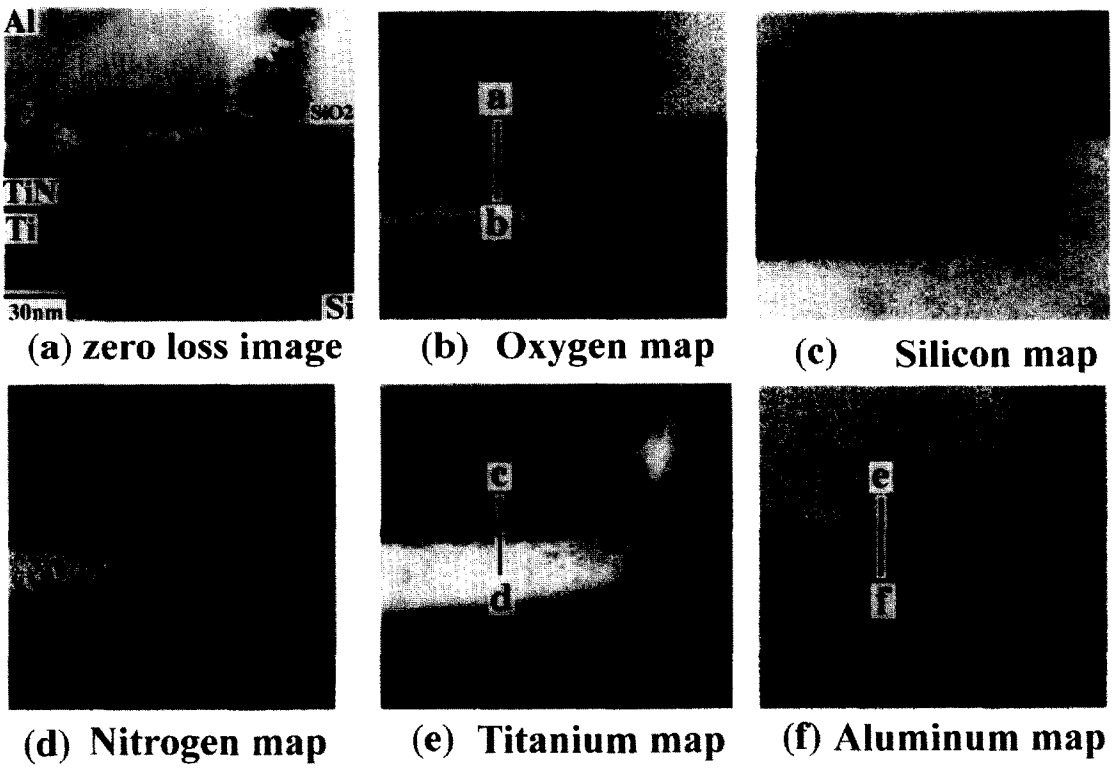

Fig. 10. (a) Zero loss image (b) O, (c) Si, (d) N, (e) Ti and (f) Al map, of a OS sample, respectively. All the images have the same magnification as shown in the zero loss image.

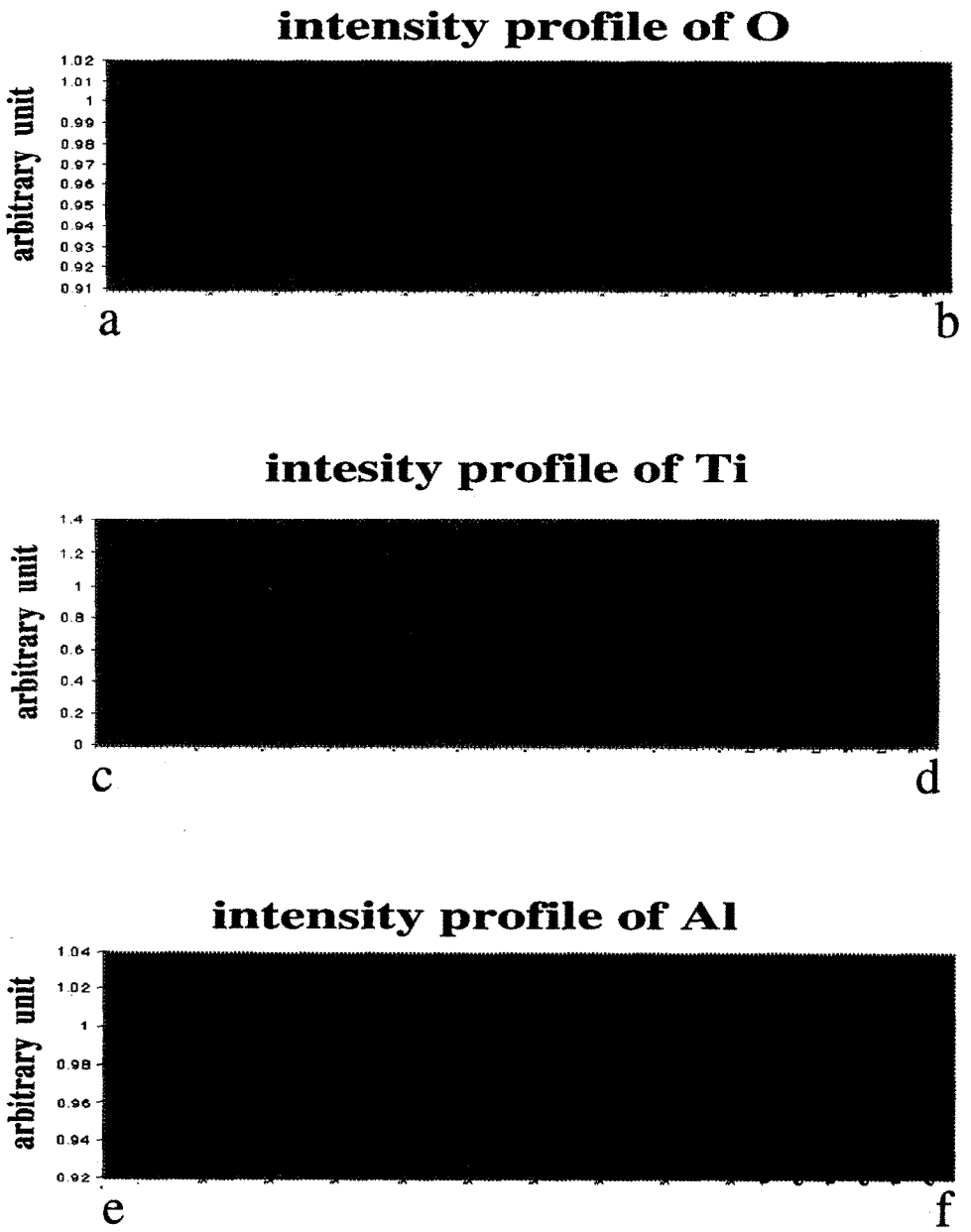

Fig. 11. Intensity profiles across the interface and contact metal/barrier for O, Al and Ti obtained from O, Al and Ti maps.

These two interfacial reactions predict the product of $TiAl_3$ as in the case of NOS samples. The contact metal lights up in both Al and Ti maps, supporting the thermodynamical calculation. The composition of the contact metal was confirmed from EDX spectra given in Fig. 11 which shows the atomic concentration ratio of Ti and Al is close to 1:3.

A previous research proposed that the spiking from the corner of contact is due to the high stress concentration at the corner [29]. In the present case, both NOS and OS processes produce devices in the same size and shape. Hence, the stress level at the corner region would not be significantly different between NOS and OS devices, even if a thin layer of titanium oxide was present in the OS case. If stress concentration was the cause, the Al spike should also be observed in OS samples. We have examined many contacts in the OS samples, no spike has been found. Therefore, the failure mechanism for NOS samples the can be concluded to be related with interfacial reaction of Al and TiN at high temperature. The formation of interfacial oxides of Ti and Al in OS samples effectively stops the interfacial reaction from TiN. Therefore, no spike was found.

4. CONCLUSION

The interfacial reaction of TiN/Ti barrier for multilayers of the Al–1%Si–0.5%Cu/TiN/Ti/Si substrate has been investigated by analytical TEM with energy filtering technique. When the non-stuffing sample is annealed, the Ti layer reacts with Si substrate into C49–$TiSi_2$ and contact Al reacts with TiN into $TiAl_3$ and AlN simultaneously. The decomposition of TiN with Al break the barrier at the weakest point of contact corner. As a result, Al leaks out from contact and diffuses along the TiN/Si interface to react with TiN again. Finally, spikes grow in the Si substrate. The mechanism for the breakdown of the TiN barrier is due to interfacial reaction. For a contact device with TiN diffusion barrier layer to survive thermal stress testing at 550°C, it is necessary to block the interfacial reaction of TiN with contact Al. Therefore, oxygen-stuffing has succeeded to prevent TiN from reacting with Al by forming a layer of titanium oxide. Furthermore, titanium oxide can react with Al at the bottom of contact to produce aluminum oxide and $TiAl_3$ during the thermal stress test, providing additional blocking structures.

Acknowledgements—The authors would like to thank the support from PVD Division, Applied Materials, U.S.A., and Materials Science Center, National Tsing Hua University.

REFERENCES

1. Learn, A. J., *J. Electrochem. Soc.*, 1975, **122**, 1127.
2. Kohlhase, A., Mandl, M. and Pamler, W., *J. Appl. Phys.*, 1989, **65**(6), 15.
3. Ting, C. Y. and Wittmer, M., *Thin Solid Films*, 1982, **96**, 327.
4. Sumi, I., Blomberg, M. and Saarilaohti, J., *J. Vac. Sci. Technol. A*, 1985, **3**, 2233.
5. Norstrom, H., Nygren, S., Wiklumd, P., Ostling, M., Buchta, R. and Petersson, C. S., *Vacuum*, 1985, **35**, 547.
6. Amigliato, A. and Valdre, G., *J. Appl. Phys.*, 1986, **61**, 61.
7. Wittmer, M., *J. Vac. Sci. Technol. A*, 1984, **2**, 273.
8. Kanamori, S., *Thin Solid Films*, 1986, **136**, 195.
9. Powell, B. D. and Mykura, H., *Acta metall.*, 1973, **21**, 1151.
10. Bernasconi, J., Strassler, S., Knecht, B., Klein, H. P. and Menth, A., *Solid State Commun.*, 1977, **21**, 867.
11. Chen, W. J. and Chen, F. R., *Philos. Mag. A*, 1993, **68**, 605.
12. Chen, F. R., Chu, C. C., Wang, J. Y. and Chang, L., *Philos. Mag.*, 1995, **72**, 529.
13. Campbell, G. H., Wein, W. L., King, W. E., Foiles, S. M. and Ruhle, M., *Ultramicroscopy*, 1993, **51**, 247.
14. Merkle, K. L. and Smith, D. J., *Ultramicroscopy*, 1987, **22**, 57.
15. Krivanek, O. L., Gubbens, A. J. and Dellby, N., *Microsc. Microanal. Microstruct.*, 1991, **2**, 315.
16. Krivanek, O. L., Gubbens, A. J., Kundmann, M. K. and Carpenter, G. C., in *Proc. 51th Annual MSA Meeting*. San Francisco Press, San Francisco, 1993, p. 586.
17. Private Communication, Applied Materials, Santa Clara, U.S.A.
18. Joy, D. C., in *Principles of Analytical Electron Microscopy*, ed. D. C. Joy, A. D. Romig, Jr. and J. I. Goldstein. Plenum, New York, 1986, p. 272.
19. Egerton, R. F., *Electron Energy-Loss Spectroscopy in the Electron Microscope*. Plenum Press, New York, 1986.
20. Zaluzec, N. J., in *Introduction to Analytical Electron Microscopy*, ed. J. J. Hren, J. I. Goldstein and D. C. Joy. Plenum, New York, 1979.
21. Goldstein, J. I., Williams, D. B. and Cligg, G., in *Princles of Analytical Electron Microscopy*, ed. D. C. Joy, A. D. Romig, Jr. and J. I. Goldstein. Plenum, New York, 1986, p. 155.
22. Villars, P. and Calvert, L. D., *Pearson's Handbook of Crystallographic Data*. ASM International, 1991.
23. Kubaschewski, O. and Alcock, C. B., *Metallurgic Thermochemistry*, 5th edn. Pergamon Press, Oxford, New York, 1979..
24. Kattner, U. R., Lin, J. C. and Chang, Y. A., *Metall. Trans. A*, 1992, **23**, 2081.
25. Grigorov, G. I., Grigorov, K. G., Stoyanova, M., Vignes, J. L., Langeron, J. P. and Denjean, P., *Appl. Phys. A*, 1993, **57**, 195.
26. Sobue, S., Mukainakano, S., Ueno, Y. and Hattori, T., *Jpn. J. Appl. Phys.*, 1995, **34**, 987.
27. Mayer, J. W., Lau, S. S., *Electronic Materials Science for Integrated Circuits in Si and GaAs*. Macmillan Publishing Company, 1990.
28. Armigliato, A. and Valdre, G., *J. Appl. Phys*, 1987, **61**, 390.
29. Private communication. Applied Materials, Santa Clara, U.S.A.